



## OPEN ACCESS

## EDITED BY

Thelma Berquo,  
Concordia College, United States

## REVIEWED BY

Daniele Thallner,  
University of Florida, United States  
Shuhui Cai,  
Chinese Academy of Sciences (CAS),  
China

## \*CORRESPONDENCE

Xiaoqiang Yang,  
✉ eesyxq@mail.sysu.edu.cn

RECEIVED 03 August 2023

ACCEPTED 02 October 2023

PUBLISHED 16 October 2023

## CITATION

Chen Q, Sun Q, Liao L, Wang W and  
Yang X (2023), Magnetic characteristics of  
Chinese archaeological bricks and their  
implications for archaeomagnetism.  
*Front. Earth Sci.* 11:1272317.  
doi: 10.3389/feart.2023.1272317

## COPYRIGHT

© 2023 Chen, Sun, Liao, Wang and Yang.  
This is an open-access article distributed  
under the terms of the [Creative  
Commons Attribution License \(CC BY\)](#).  
The use, distribution or reproduction in  
other forums is permitted, provided the  
original author(s) and the copyright  
owner(s) are credited and that the original  
publication in this journal is cited, in  
accordance with accepted academic  
practice. No use, distribution or  
reproduction is permitted which does not  
comply with these terms.

# Magnetic characteristics of Chinese archaeological bricks and their implications for archaeomagnetism

Qiong Chen<sup>1</sup>, Qirui Sun<sup>2</sup>, Lishan Liao<sup>1</sup>, Wei Wang<sup>1</sup> and  
Xiaoqiang Yang<sup>3\*</sup>

<sup>1</sup>Joint International Research Laboratory for Environmental and Social Archaeology, Institute of Cultural Heritage, Shandong University, Qingdao, China, <sup>2</sup>Shandong Institute of Cultural Relics and Archaeology, Jinan, China, <sup>3</sup>School of Earth Science and Engineering, Sun Yat-sen University, Zhuhai, China

Fired archaeological objects have been widely studied in palaeomagnetic research. However, the uneven heating during the firing process can affect the type, grain size and magnetic domain characteristics of the magnetic carrier, which in turn can lead to notable discrepancies in the paleomagnetic information that they captured. In this study, we conducted a detailed rock magnetic study on two Chinese archaeological (one grey and one red) to reveal the properties of magnetic minerals subjected to different firing temperatures. Our results show that single domain (SD) magnetite with strong magnetostatic interactions is the dominant magnetic carrier in grey bricks, while SD magnetite with weak magnetostatic interactions is the dominant magnetic carrier in the red bricks. And stepwise heating results show that the firing temperature of the grey brick and the outer layers of red brick (R-1, R-3) is above 700°C, while the inner layer (R-2) of red brick shows a thermal transformation process at ~350°C. This uneven heating may cause the spatial discrepancies in magnetic parameters such as the mass-normalized magnetic susceptibility ( $\chi$ ) and natural remanent magnetization (NRM) in red brick. Nevertheless, the direction of the geomagnetic field can be accurately obtained even if the brick is not heated evenly. However, more work is needed to explore the paleointensity behavior at different firing temperatures.

## KEYWORDS

archaeomagnetism, fired brick, rock magnetism, China, magnetic properties

## 1 Introduction

A large amount of archaeological geomagnetic data has been reported in recent decades, and has contributed significantly to the recovery of the secular variation of the geomagnetic field over the last 10,000 years (e.g., Ben-Yosef et al., 2009; Cai et al., 2017; 2020; Mahgoub et al., 2019). Fired archaeological objects, such as pottery, baked brick, burnt clay, and slags, can acquire thermoremanent magnetization (TRM) during the firing process, and have been widely used in paleomagnetism studies (Brown et al., 2015). However, these archaeological geomagnetic samples were mostly taken from kilns and hearths, and might have experienced uneven heating due to the fact that the heating temperatures of the various parts of the kiln and hearths can vary significantly. For example, Wei et al. (1980) found that the kiln floor and the outer layer of the kiln wall (1–4 cm thick) at the Jiangzhai site in China were subjected to higher heat, usually above 800°C, while the burnt soil in the inner layer have

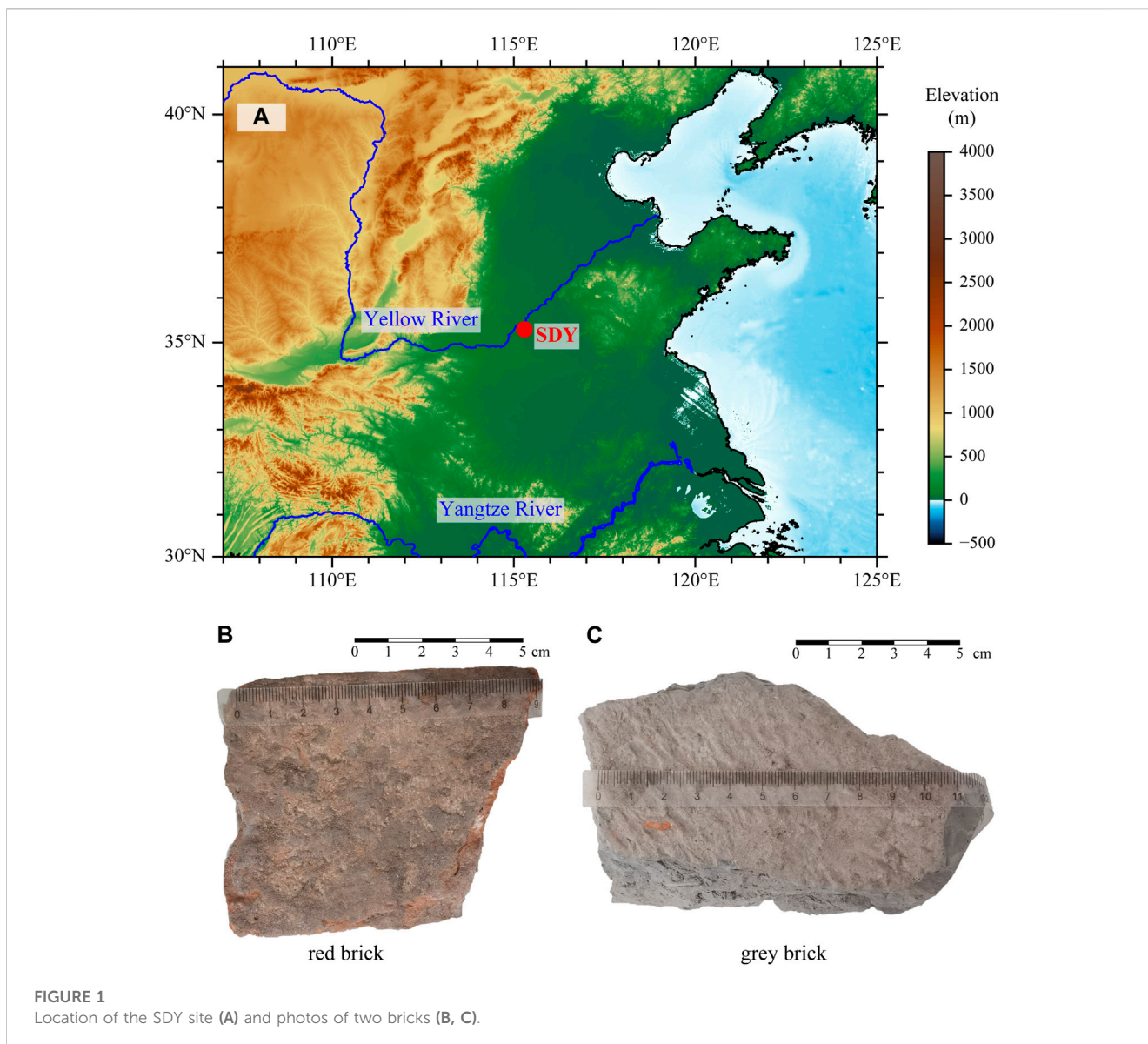


**FIGURE 1**  
Location of the SDY site (A) and photos of two bricks (B, C).

been exposed to a temperature of 400°C. The main magnetic carriers in archaeomagnetic materials are transformed from other minerals during the firing process. Therefore, the uneven heating due to firing temperature differences may have affected the type, grain size, and magnetic domain characteristics of the magnetic carrier, ultimately affecting the paleomagnetic information. There is limited research on the thermal properties of fired archaeological objects and their magnetic properties, which hinders our understanding of archaeological geomagnetism.

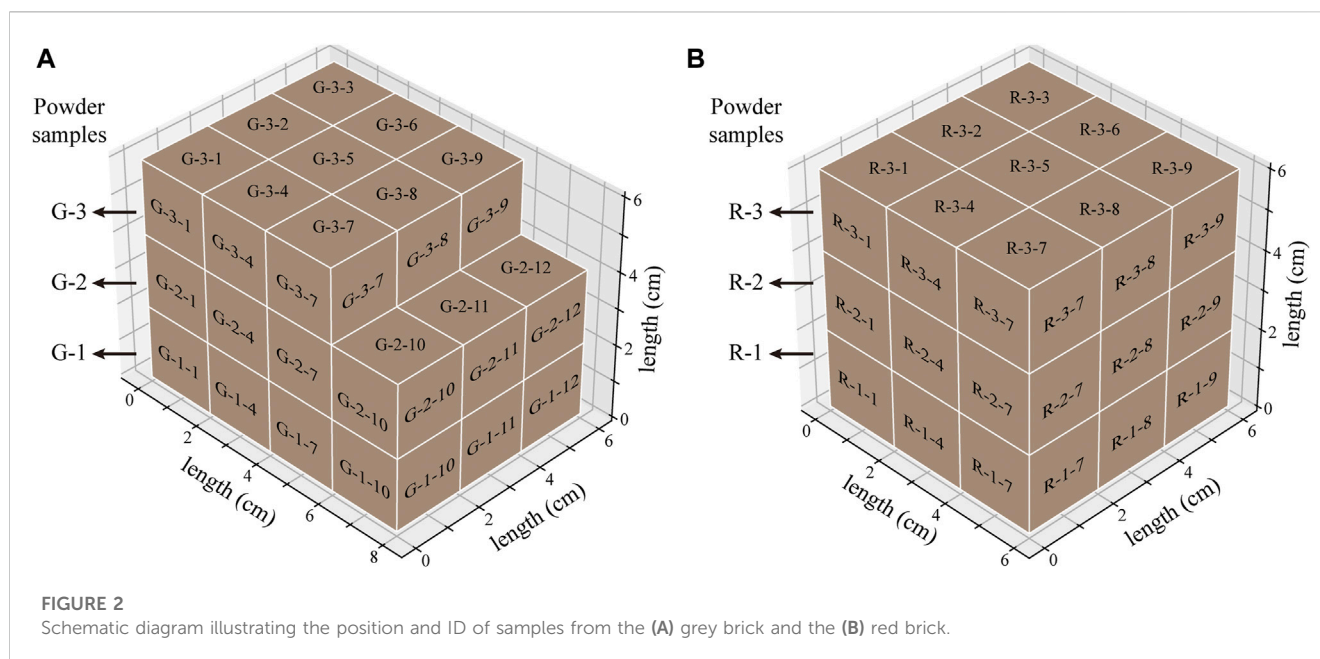
Among the various fired archaeological objects, baked bricks are more susceptible to uneven heating due to their thickness. In ancient China, the use of baked bricks dates back to the Yangshao culture, and they were widely produced and utilized during the Warring States Period and Qin-Han Dynasties (Yang et al., 2014). And, specialized kilns were developed for firing these bricks during the Han Dynasty, indicating the advanced state of firing technology at that time. Therefore, conducting rock magnetic analysis on Han dynasty bricks can provide insight into the effect of firing

temperature on the magnetic characteristics of archaeological geomagnetic materials. Towards this end, we conducted a detailed rock magnetic study on two ancient Chinese bricks dating back to the Han Dynasty.

## 2 Materials and methods

Fragments from two bricks, one red and one grey, were collected from brick tombs at the Sundayuan archaeological site in Shandong Province, China (Figure 1). The red brick can be traced back to the Western Han Dynasty, while the grey brick belongs to the Eastern Han Dynasty. Their lengths are 9.1 cm and 12.0 cm, respectively, and their thicknesses are between 6.4 and 6.6 cm. When observed under a microscope, the red brick exhibits a loose texture with more visible pores, while the grey brick appears denser.

A diamond wire cutter was used to cut approximately 3 mm from each side of the bricks to expose the inner surface and eliminate



the influence of the soil contaminants after burial. The remaining bricks were cut into three layers at approximately 2 cm intervals along the cut surface, and were then cut into 2×2×2 cm cubic samples (Figure 2) such that a total of 60 cubic samples were obtained. These cubic samples were numbered and marked with their location information. In addition, the remaining part of each layer was ground into powder for magnetic analysis, and a total of 6 powder samples (3 layers per brick) were obtained.

The mass-normalized magnetic susceptibility ( $\chi$ ) and natural remanent magnetization (NRM) of all cubic samples were measured using the Kappabridge-MFK2 at a frequency of 976 Hz and the Spinner Magnetometer (JR-6A, AGICO Co. Ltd.), respectively. Stepwise alternating field (AF) demagnetization was conducted on even numbered cubic samples using the LDA5 AF demagnetizer, and was carried out at 5 mT steps for the 0–100 mT interval, and at 10 mT steps from 100 to 150 mT. Stepwise thermal demagnetization was conducted on odd numbered cubic samples using an ASC TD-48 thermal demagnetizer in 50°C steps from 50°C to 700°C. Remanent demagnetization and direction were measured on JR-6A after each demagnetization step. Anhyseretic remanent magnetization (ARM), isothermal remanent magnetization (IRM), hard isothermal remanent magnetization (HIRM), S-ratio were obtained from the following procedures after AF demagnetization. ARM was imparted in a 100 mT alternating field with a superimposed 50  $\mu$ T direct bias field using the LDA5 AF demagnetizer and pluse magnetizer (PAM1). A saturation IRM was imparted in a 1 T applied field, termed SIRM, then samples were demagnetized with backfields of –300 mT, and the corresponding remanence were measured and termed IRM<sub>-300mT</sub>. HIRM is defined as  $0.5 \times (\text{SIRM} + \text{IRM}_{-300\text{mT}})$  and the S-ratio is defined as  $-\text{IRM}_{-300\text{mT}}/\text{SIRM}$ . The ratios of ARM/SIRM and HIRM/SIRM are calculated. The former is commonly used as a grain-size indicator for magnetic minerals. The latter is similar to S-ratio and commonly used to estimate the relative abundance variations of ferrimagnetic and

antiferromagnetic minerals. The temperature-dependent of magnetic susceptibility ( $\chi$ -T) of powdered samples was investigated using the secondary heating method and the stepwise heating method, respectively. In the secondary heating method, the heated samples underwent a second  $\chi$ -T cycle after the initial  $\chi$ -T cycle. In the stepwise heating method, the maximum temperature of each cycle was gradually increased from 100°C to 700°C in 50°C steps. All  $\chi$ -T measured using a Kappabridge-MFK2 system in an argon environment at a 976 Hz frequency. Hysteresis loops were measured to maximum applied fields of 1 T using a vibrating sample magnetometer (VSM, Princeton MicroMag 3900) at room temperature. Saturation magnetization ( $M_s$ ), saturation remanent magnetization ( $M_{rs}$ ), and coercivity ( $B_c$ ) were obtained after high-field slope correction. The remanence coercivity ( $B_{cr}$ ) was obtained from back-field demagnetization curves of 0 T back to –1 T. IRM acquisition curves with 100 measurement points and nonlinear field steps on a log scale up to 1 T were measured using the VSM. The IRM acquisition curves were decomposed into magnetic components using the method described in Maxbauer et al. (2016). First-order reversal curve (FORC) with 120 FORC were also measured using the VSM for powder samples, and FORC diagrams were processed using the FORCinel version 3.06 software from Harrison and Feinberg (2008).

The sample preparation, AF demagnetization experiments, and  $\chi$ -T curve experiments were carried out at the Archaeological Geomagnetic Laboratory at Shandong University, and the rest of the experiments were carried out at the Magnetism Laboratory at Sun Yat-sen University.

### 3 Results

For the grey brick samples,  $\chi$  ranged from 4.5 to 6 ( $\times 10^{-7}$  m<sup>3</sup>/kg), and the NRM ranged from 35 to 50 ( $\times 10^{-5}$  Am<sup>2</sup>/kg) (Supplementary Table S1). The  $\chi$  and NRM of red brick samples were one order of

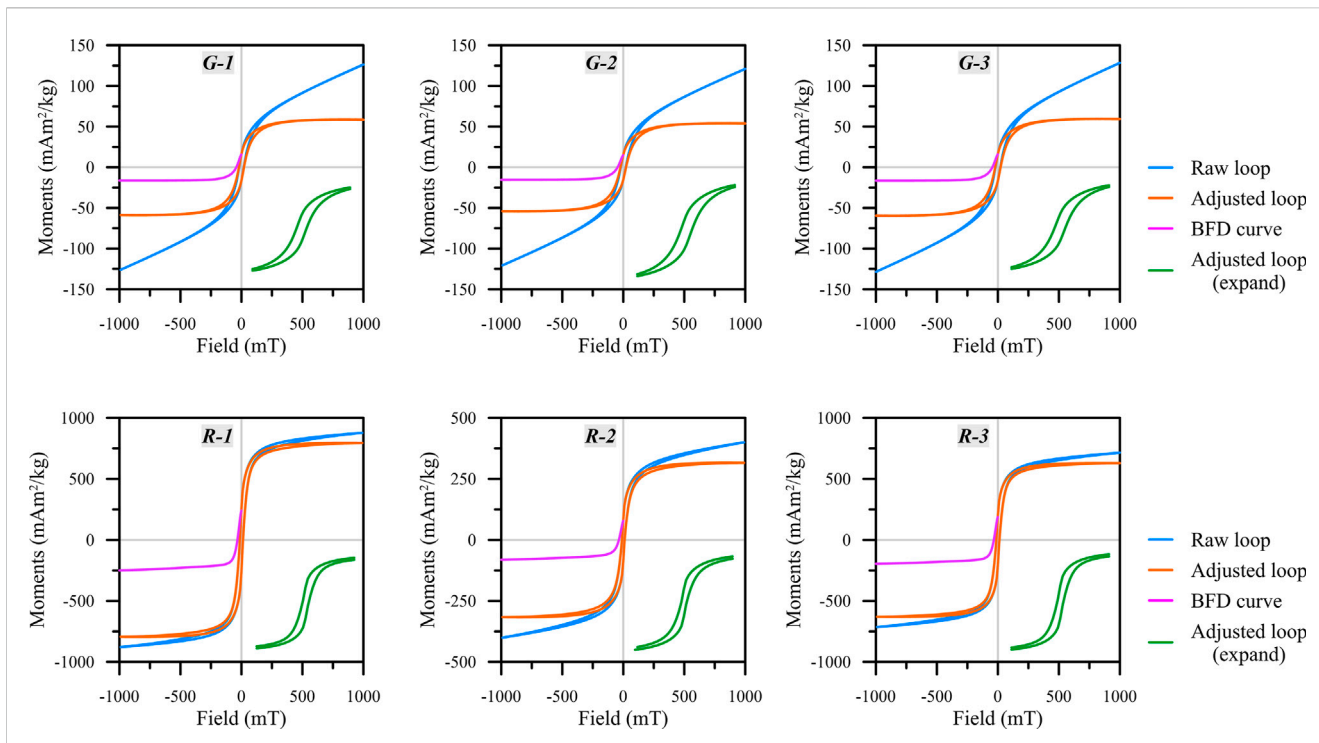


**FIGURE 3**  
 Hysteresis loops and back-field demagnetization curves of representative samples. The blue lines are raw loops, orange lines are adjusted loops by paramagnetic correction, magenta lines are back-field demagnetization curves, and green lines are the amplified plot of adjusted loop between  $-200$  mT and  $200$  mT.

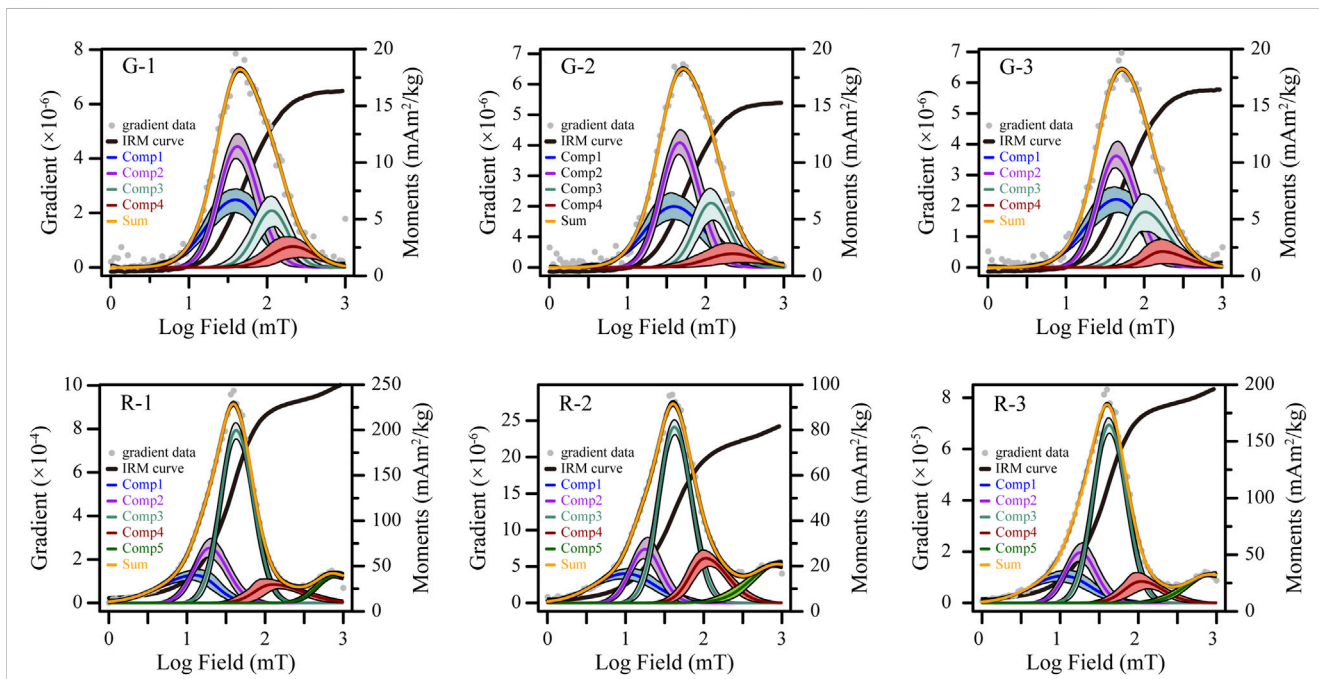
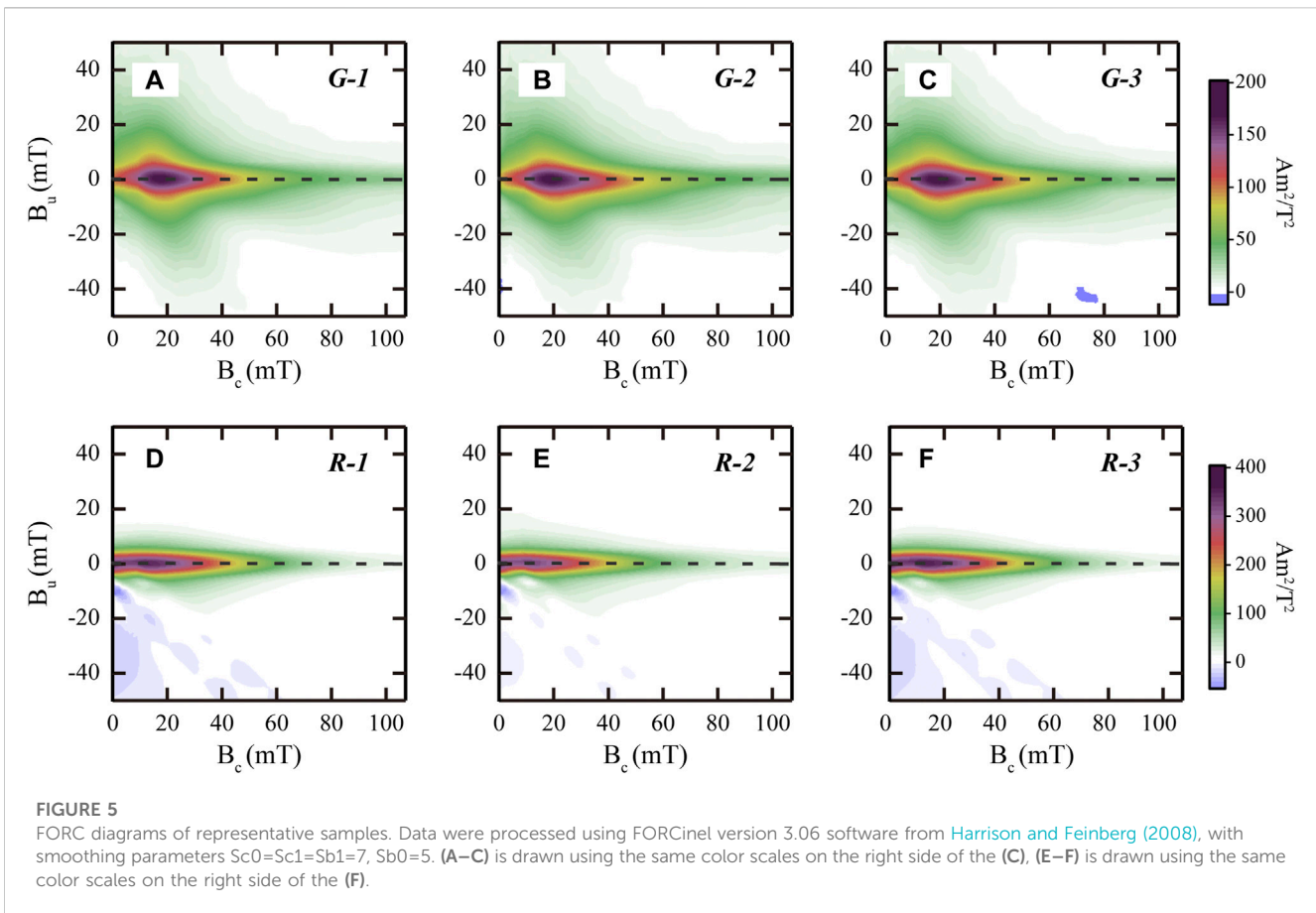


**FIGURE 4**  
 IRM unmixing results of representative samples. Black lines are raw data, gray dots are gradient data, orange lines are the sum of components, and other color lines are individual components.



magnitude higher than those of grey brick; the  $\chi$  ranged from 40 to 170 ( $\times 10^{-7}$  m<sup>3</sup>/kg), and the NRM was ranged from 75 to 600 ( $\times 10^{-5}$  Am<sup>2</sup>/kg) (Supplementary Table S1).

Hysteresis loops for all powdered samples are closed below 0.3 T (Figure 3), which indicates a dominance of magnetically soft ferrimagnetic minerals (Dunlop, 2002). Grey brick samples show “potbellied” loops with  $B_c$  ranging between 20.5 mT and 22.5 mT, and  $B_{cr}$  ranging between 42 mT and 47 mT (Figures 3A–C). Red brick samples show “wasp-waisted” loops with  $B_c$  ranging between 10 mT and 12 mT, and  $B_{cr}$  ranging between 33 mT and 36 mT (Figures 3D–F).

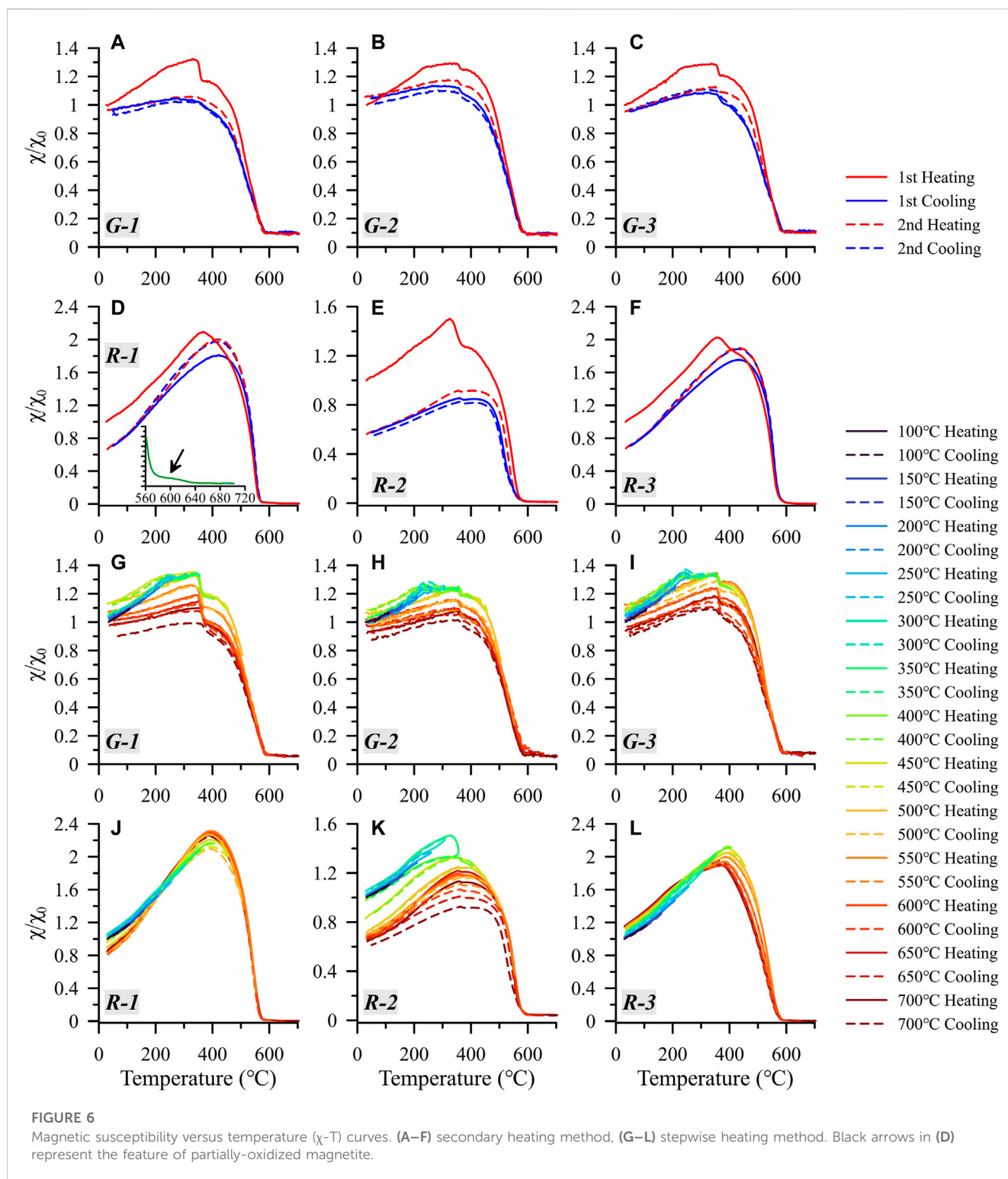
IRM acquisition curves can be used to decomposed into magnetic mineral components based on coercivity spectra (Heslop et al., 2002). In general, four components are recognized for grey brick, and five components for red brick (Figure 4; Supplementary Table S2). In grey brick, components 1 ( $B_{1/2} = 37.82\text{--}41.6$  mT, DP = 0.36) and 2 ( $B_{1/2} = 43.89\text{--}47.77$  mT, DP = 0.25) are major remanence carriers, which were interpreted as magnetite/maghemite (Wang et al., 2022). Component 3 ( $B_{1/2} = 113.49\text{--}121.95$  mT, DP = 0.21–0.25) was interpreted as partially-oxidized coarse-grained magnetite. Finally, component 4 ( $B_{1/2} = 208.92\text{--}231.52$  mT, DP = 0.25–0.33) is attributed to antiferromagnetic hematite (Heslop et al., 2002).

In red brick, components 1 ( $B_{1/2} = 9.08\text{--}9.61$  mT, DP = 0.15) and 2 ( $B_{1/2} = 18.09\text{--}20.39$  mT, DP = 0.14–0.18) likely represents the coarse-gained magnetite (Roberts et al., 2011). Component 3 ( $B_{1/2} = 43.39\text{--}44.17$  mT, DP = 0.2) is a major remanence carrier and was

interpreted as magnetic/maghemite. Components 4 ( $B_{1/2} = 122.73\text{--}169.73$  mT, DP = 0.24–0.3) and 5 ( $B_{1/2} = 954.38\text{--}1015.62$  mT, DP = 0.3–0.37) were interpreted as the same as grey brick components 3 and 4, respectively. In addition, the difference of IRM acquisition curves at high fields for the two types of brick also suggest the presence of considerable amounts of hematite in the red brick.

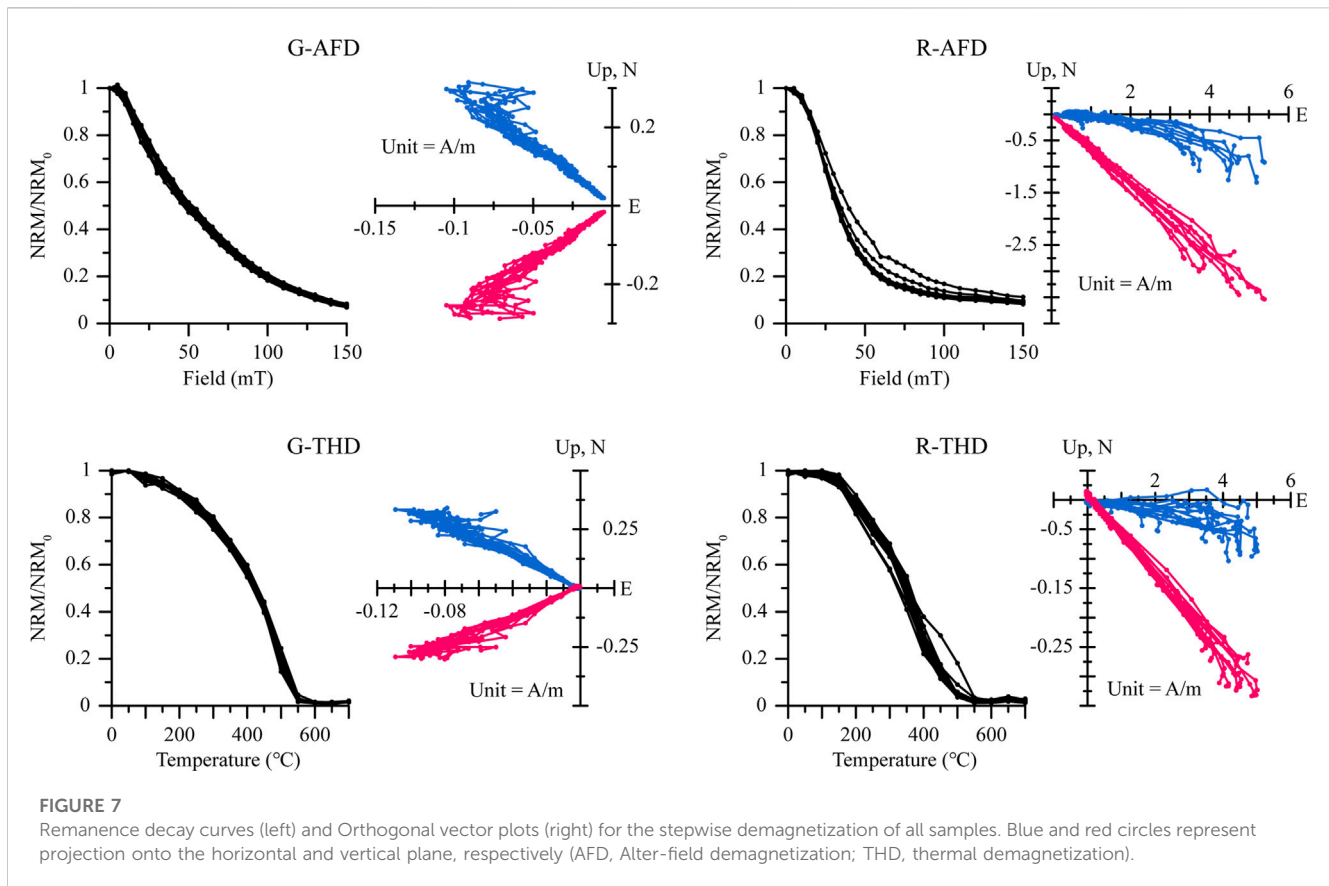
FORC diagrams were used to identify and discriminate among different components in a mixed magnetic mineral assemblage (Figure 5; Pike et al., 1999; Roberts et al., 2000). FORC diagrams for samples from grey brick were characterized by concentric distribution with moderate vertical spread, which indicate the presence of single domain (SD) particles with strong magnetostatic interactions (Figure 5; Roberts et al., 2017; Roberts et al., 2000). The FORC diagrams for red brick are elongated contours along the horizontal axis with small vertical spread. Red brick FORC diagrams also contain a secondary peak near the origin of the diagram, which indicate the presence of weak-interacting SD particles and SP particles (Figure 5; Roberts et al., 2017).

$\chi$ -T curves are sensitive to magnetic mineralogical changes during thermal treatment, which can provide information about magnetic mineralogy (Deng et al., 2001). All heating curves are characterized by a marked drop at 585°C, the Curie temperature of magnetite, which demonstrates that magnetite is the dominant magnetic minerals in both bricks (Figure 6). The heating curve of red brick is still decreasing after 585°C, indicating the presence of partially-oxidized magnetite or hematite which also corresponding



with the decomposition results of IRM. The steady increase of  $\chi$  below approximately 250°C is interpreted as the unblocking of fine-grained ferrimagnetic particles. In the grey brick, a significant decrease of  $\chi$  can be observed between 350°C and 360°C, but this decrease is reversible and can be observed in stepwise  $\chi$ -T (Figure 6). This reversal change is not caused by the transformation of the mineral. It is most likely due to the changes of magnetic interactions during heating. For an SD particle with strong interaction, the

interaction will first decrease and then increase during heating, which may affect the susceptibility characteristics at high temperature (Carvallo et al., 2004; Dodrill et al., 2015). For the R-2 samples in red brick, the decrease of  $\chi$  between approximately 300°C and 360°C is irreversible, suggesting that the decrease of  $\chi$  might be caused by the transformation of maghemite to hematite. In addition, almost all heating curves are higher than cooling curves, possibly due to the loss or oxidation of the magnetite and the



transformation of ferromagnetic maghemite to antiferromagnetic hematite during heating (Liu et al., 2003; Zhang and Appel, 2023). In the secondary  $\chi$ -T cycle and stepwise  $\chi$ -T cycle, the  $\chi$ -T curves of G-1, G-2, G-3, R-1 and R-3 are reversible, indicating the firing temperature of two bricks are high than 700°C. The presence of maghemite in the R-2 samples indicates that the firing temperature is unexpectedly below 350°C. It is surprising to see such a low temperature in the middle layer of a brick with a thickness of ~6.4 cm. This is probably due to the short firing time at high temperature in kiln. Even though the initial firing temperature of the middle layer might have been higher, possibly exceeding 700°C, the short firing time may have led to incomplete transformation of the minerals. Overall, the significantly low values of  $\chi$ , NRM and  $M_s$  of R-2 suggest that the red brick is heated unevenly (Supplementary Tables S1, S3; Figure 3).

Orthogonal vector demagnetization plots (Zijderveld, 2013) and NRM decay diagrams for all samples are shown in Figure 7. The viscous remanent magnetization (VRM), which is acquired by large-sized, MD grains during transportation, storage, or preparation, can be progressively removed after 0–15 mT/100°C demagnetization. After VRM is removed, all samples showed a stable decay-to-origin component up to 150 mT/600°C, which was interpreted as the characteristic remanent magnetization (ChRM) of the samples. The NRM directions were determined using principal component analysis (PCA) for the linear part of ChRM, generally between 20 and 100 mT and 150°C–550°C. The direction obtained by AF and thermal demagnetization are the same for both bricks. Based on the magnetic and demagnetization results, we interpreted the ChRM of

the grey brick to be dominantly carried by SD magnetite with strong magnetostatic interactions, and for the red brick by SD magnetite/maghemite with weak magnetostatic interactions.

## 4 Discussion

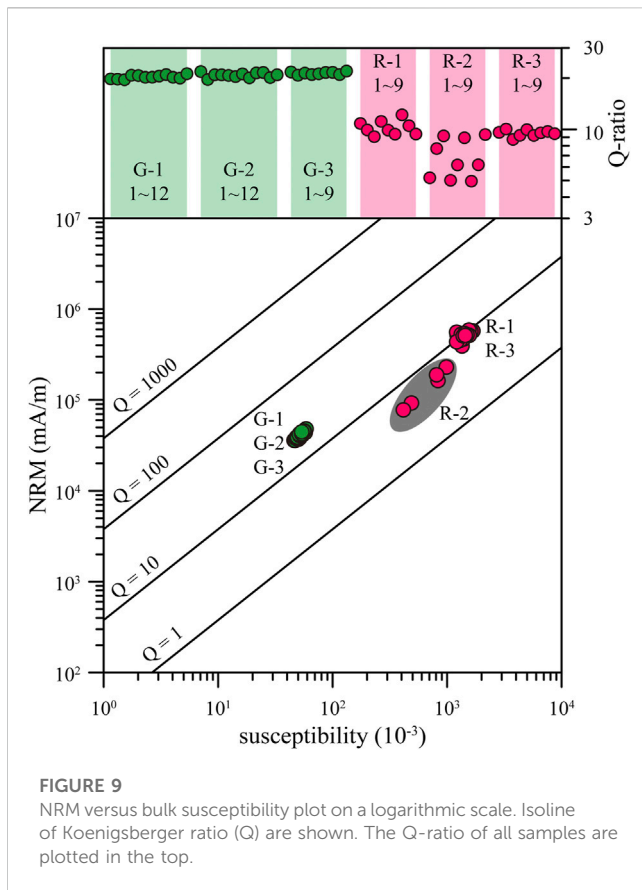
### 4.1 Spatial characteristics of rock magnetism in brick

The spatial distribution of the  $\chi$  and NRM of the two bricks analyzed in this study is shown in Figure 8. In these figures, we see that the red brick shows significant spatial heterogeneity in  $\chi$  and NRM, mainly in the second layer where the values are significantly lower than other layers (Figures 8B, D). The value ranking of  $\chi$  and NRM of the red brick's three layers are as follow: first layer  $\approx$  third layer  $\gg$  second layer. The grey brick, on the other hand, does not show any significant spatial differences (Figures 8A, C). According to the results of rock magnetism, the main reason for this difference in spatial distribution is related to the original firing temperature.

The first and third layers of red brick shows reversible heating and cooling curves with a 20% decrease in  $\chi$  after cooling to room temperature. This indicates that the magnetite was oxidized during heating. The second layer had an irreversible behavior with a 45%–55% decrease in  $\chi$  after cooling, and a decrease between approximately 300°C and 360°C of the heating curve, which shows the thermal characteristics of maghemite and magnetite. While the presence of maghemite does not indicate that the







size of magnetic mineral between different layers are further manifested as the spatial heterogeneity in the magnetic parameters ( $\chi$  and NRM).

In addition to  $\chi$  and NRM, the above spatial heterogeneity is also observed in other parameters. For example, the values of  $M_s$  and  $M_{rs}$  of the second layer in the red brick is significantly lower than other layers (Figure 3; Supplementary Table S3). In the coercivity spectra, the contribution of component 4 (partially-oxidized coarse-grained magnetite) in the second layer (~14%) is higher than in other layers (~7%). However, there is no obvious difference in the  $B_c$  and  $B_{cr}$  of the three layers of the red brick, and the FORC diagram shows similar characteristics.

## 4.2 Implications for archaeomagnetism

Brick and other fired archaeological artifacts (e.g., pottery, metallurgical slags, and kiln fragments) are favorable materials to recover the secular variation of the Earth's magnetic field in archaeomagnetism research (Cai et al., 2017; Mahgoub et al., 2019; Wang et al., 2023). However, it is rare to obtain full vector information (both direction and paleointensity) of the Earth's magnetic field due to the difficulty in preserving these materials *in situ*. In this study, the direction obtained from different positions of brick by different demagnetization method is similar. This suggests that the direction of the geomagnetic field can be accurately recorded even if the brick is not heated evenly. However, great caution is needed in using them to represent

paleomagnetic directions, as those bricks were moved and rotated after firing.

In the analysis of paleointensity, ideal artifacts for analysis should possess non-interacting SD particles, as only non-interacting SD grains obey the Thellier laws of additivity, reciprocity, and independence (Dunlop and Özdemir, 2001; Dunlop, 2011). However, the magnetic minerals in natural materials have different sizes, shapes, and magnetic domains, which will have non-negligible effects on the results of paleointensity analyses (Levi, 1977; Xu and Dunlop, 2004; Dunlop, 2011). For example, the Arai plot, which used to calculate the paleointensity, shows that as the grain size increases, the plot will deviate more and more from the ideal SD line. This deviation leads to an underestimation of the true paleomagnetic field strength (Dunlop, 2011; Smirnov et al., 2017). Therefore, several parameters can be used to select the most suitable samples for paleointensity experiments. The Koenigsberger ratio (Q-ratio) is an appropriate parameter to distinguish well-heated samples from those that were not sufficiently heated to carry a complete TRM (Schnepp et al., 2004; 2020a; 2020b). In this study, grey brick has a higher Q-ratio than red brick, and the Q-ratio of R-2 is significantly lower than R-1 and R-3 (Figure 9). The rock magnetic results show that the magnetic mineral particles of grey brick are coarser (lower ARM/SIRM; Supplementary Table S4) and have strong interactions. Although the red brick shows weak interaction between particles, R-2 contains higher coercivity minerals (lower S-ratio and higher HIRM/SIRM; Supplementary Table S4) and grain size is coarser than R-1 and R-3. Since paleointensity experiments were not performed in this study, according to the results of magnetism and the requirements of paleointensity theory, we speculate that the grey brick and R-2 are probably not ideal materials for paleointensity study. The differences in paleointensity information recorded in the unevenly heated samples need to be further studied.

## 5 Conclusion

In this paper, we carried out a detailed rock magnetic study on two archaeological bricks from Sundayuan site, China. Our results suggest that the dominant magnetic carrier in grey bricks is SD magnetite with strong magnetostatic interactions, while the SD magnetite in red brick is weak magnetostatic interactions. Compared with the grey brick, the red brick showed significant variations in its magnetic properties ( $\chi$  and NRM) among the three layers analyzed. These variations could be caused by differences in firing temperature and residence time of the brick in the kiln. The results of stepwise  $\chi$ -T confirmed that the firing temperature of surface layer is higher than internal layer of red brick. Our work suggests that the layers of red brick with well-heated might more suitable for paleointensity study, whereas the insufficiently heated layer of red brick and the grey brick with strong magnetic interaction are not ideal materials for paleointensity study.

Based on our findings, we recommend that future archaeomagnetism research should evaluate the  $\chi$ , NRM and Q-ratio of artifacts before carrying out any paleointensity

analyses. These tests are time-saving compared to other rock magnetism analyses (e.g.,  $\chi$ -T, loop, FORC). Combined with representative samples' rock magnetism data, the suitable samples with sufficiently heated can be effectively selected. This is very useful for paleomagnetic experiments with very large numbers of samples.

## Data availability statement

Paleomagnetic data have been deposited in the Magnetism Information Consortium (MagIC) database (DOI: [10.7288/V4/MAGIC/19925](https://doi.org/10.7288/V4/MAGIC/19925)).

## Author contributions

QC: Writing—original draft, Funding acquisition. QS: Funding acquisition, Investigation, Writing—review and editing. LL: Data curation, Writing—review and editing. WW: Funding acquisition. XY: Conceptualization, Writing—review and editing.

## Funding

The author(s) declare financial support was received for the research, authorship, and/or publication of this article. This research is supported by the projects of Social Science Foundation of Shandong Province of China (2022-JCLS-03), National Natural Science Foundation of China (41904068), Major Program of National Social Science Foundation of China (20&ZD246).

## References

- Ben-Yosef, E., Tauxe, L., Levy, T. E., Shaar, R., Ron, H., and Najjar, M. (2009). Geomagnetic intensity spike recorded in high resolution slag deposit in Southern Jordan. *Earth Planet. Sci. Lett.* 287 (3), 529–539. doi:10.1016/j.epsl.2009.09.001
- Brown, M. C., Donadini, F., Korte, M., Nilsson, A., Korhonen, K., Lodge, A., et al. (2015). GEOMAGIA50.v3: 1. general structure and modifications to the archeological and volcanic database. *Earth, Planets Space* 67 (1), 83. doi:10.1186/s40623-015-0232-0
- Cai, S., Jin, G., Tauxe, L., Deng, C., Qin, H., Pan, Y., et al. (2017). Archaeointensity results spanning the past 6 kiloyears from eastern China and implications for extreme behaviors of the geomagnetic field. *Proc. Natl. Acad. Sci.* 114 (1), 39–44. doi:10.1073/pnas.1616976114
- Cai, S., Tauxe, L., Wang, W., Deng, C., Pan, Y., Yang, L., et al. (2020). High-fidelity archeointensity results for the late neolithic Period from Central China. *Geophys. Res. Lett.* 47 (10), e2020GL087625. doi:10.1029/2020GL087625
- Carvallo, C., Özdemir, Ö., and Dunlop, D. J. (2004). First-order reversal curve (FORC) diagrams of elongated single-domain grains at high and low temperatures. *J. Geophys. Res. Solid Earth* 109 (B4). doi:10.1029/2003JB002539
- Deng, C., Zhu, R., Jackson, M. J., Verosub, K. L., and Singer, M. J. (2001). Variability of the temperature-dependent susceptibility of the Holocene eolian deposits in the Chinese loess plateau: a pedogenesis indicator. *Phys. Chem. Earth, Part A Solid Earth Geodesy* 26 (11), 873–878. doi:10.1016/S1464-1895(01)00135-1
- Doddrill, B. C., Lindemuth, J. R., Radu, C., and Reichard, H. S. (2015). White Paper: high-temperature FORC study of single- and multi-phase permanent magnets. *MRS Bull.* 40 (11), 903–905. doi:10.1557/mrs.2015.290
- Dunlop, D. J., and Özdemir, Ö. (2001). Beyond Néel's theories: thermal demagnetization of narrow-band partial thermoremanent magnetizations. *Phys. Earth Planet. Interiors* 126 (1), 43–57. doi:10.1016/S0031-9201(01)00243-6
- Dunlop, D. J. (2011). Physical basis of the Thellier–Thellier and related paleointensity methods. *Phys. Earth Planet. Interiors* 187 (3), 118–138. doi:10.1016/j.pepi.2011.03.006
- Dunlop, D. J. (2002). Theory and application of the Day plot ( $M_r/M_s$  versus  $H_{cr}/H_c$ ). 1. Theoretical curves and tests using titanomagnetite data. *J. Geophys. Res. Solid Earth* 107 (B3). doi:10.1029/2001JB000486
- Harrison, R. J., and Feinberg, J. M. (2008). FORCinel: an improved algorithm for calculating first-order reversal curve distributions using locally weighted regression smoothing. *Geochem. Geophys. Geosystems* 9 (5). doi:10.1029/2008GC001987
- Heslop, D., Dekkers, M. J., Kruiver, P. P., and Van Oorschot, I. H. M. (2002). Analysis of isothermal remanent magnetization acquisition curves using the expectation-maximization algorithm. *Geophys. J. Int.* 148 (1), 58–64. doi:10.1046/j.0956-540x.2001.01558.x
- Kreimeyer, R. (1987). Some notes on the firing colour of clay bricks. *Appl. Clay Sci.* 2 (2), 175–183. doi:10.1016/0169-1317(87)90007-X
- Levi, S. (1977). The effect of magnetite particle size on paleointensity determinations of the geomagnetic field. *Phys. Earth Planet. Interiors* 13 (4), 245–259. doi:10.1016/0031-9201(77)90107-8
- Liu, Q., Banerjee, S. K., Jackson, M. J., Chen, F., Pan, Y., and Zhu, R. (2003). An integrated study of the grain-size-dependent magnetic mineralogy of the Chinese loess/paleosol and its environmental significance. *J. Geophys. Res. Solid Earth* 108 (B9). doi:10.1029/2002JB002264
- Mahgoub, A. N., Juárez-Arriaga, E., Böhnell, H., Manzanilla, L. R., and Cyphers, A. (2019). Refined 3600 years palaeointensity curve for Mexico. *Phys. Earth Planet. Interiors* 296, 106328. doi:10.1016/j.pepi.2019.106328
- Maritan, L., Nodari, L., Mazzoli, C., Milano, A., and Russo, U. (2006). Influence of firing conditions on ceramic products: experimental study on clay rich in organic matter. *Appl. Clay Sci.* 31 (1), 1–15. doi:10.1016/j.clay.2005.08.007
- Maxbauer, D. P., Feinberg, J. M., and Fox, D. L. (2016). MAX UnMix: a web application for unmixing magnetic coercivity distributions. *Comput. Geosciences* 95, 140–145. doi:10.1016/j.cageo.2016.07.009

## Acknowledgments

The authors thank two reviewers for their helpful and constructive reviews of the manuscript. We thank LetPub ([www.letpub.com](http://www.letpub.com)) for linguistic assistance and pre-submission expert review and we are grateful to Wanyun Liu for assisting in the analysis of the thermal demagnetization. QC acknowledges the support of the Yale MacMillan Center for inviting her to the Yale University.

## Conflict of interest

The authors declare that the research was conducted in the absence of any commercial or financial relationships that could be construed as a potential conflict of interest.

## Publisher's note

All claims expressed in this article are solely those of the authors and do not necessarily represent those of their affiliated organizations, or those of the publisher, the editors and the reviewers. Any product that may be evaluated in this article, or claim that may be made by its manufacturer, is not guaranteed or endorsed by the publisher.

## Supplementary material

The Supplementary Material for this article can be found online at: <https://www.frontiersin.org/articles/10.3389/feart.2023.1272317/full#supplementary-material>

- Pérez-Monserrat, E. M., Maritan, L., Garbin, E., and Cultrone, G. (2021). Production technologies of ancient bricks from padua, Italy: changing colors and resistance over time. *Minerals* 11 (7), 744. doi:10.3390/min11070744
- Pike, C. R., Roberts, A. P., and Verosub, K. L. (1999). Characterizing interactions in fine magnetic particle systems using first order reversal curves. *J. Appl. Phys.* 85 (9), 6660–6667. doi:10.1063/1.370176
- Roberts, A. P., Almeida, T. P., Church, N. S., Harrison, R. J., Heslop, D., Li, Y., et al. (2017). Resolving the origin of pseudo-single domain magnetic behavior. *J. Geophys. Res. Solid Earth* 122 (12), 9534–9558. doi:10.1002/2017JB014860
- Roberts, A. P., Florindo, F., Villa, G., Chang, L., Jovane, L., Bohaty, S. M., et al. (2011). Magnetotactic bacterial abundance in pelagic marine environments is limited by organic carbon flux and availability of dissolved iron. *Earth Planet. Sci. Lett.* 310 (3), 441–452. doi:10.1016/j.epsl.2011.08.011
- Roberts, A. P., Pike, C. R., and Verosub, K. L. (2000). First-order reversal curve diagrams: a new tool for characterizing the magnetic properties of natural samples. *J. Geophys. Res. Solid Earth* 105 (B12), 28461–28475. doi:10.1029/2000JB900326
- Schnepf, E., Pucher, R., Reinders, J., Hambach, U., Soffel, H., and Hedley, I. (2004). A German catalogue of archaeomagnetic data. *Geophys. J. Int.* 157 (1), 64–78. doi:10.1111/j.1365-246X.2004.02163.x
- Schnepf, E., Thallner, D., Arneitz, P., and Leonhardt, R. (2020a). New archeomagnetic secular variation data from Central Europe, II: intensities. *Phys. Earth Planet. Interiors* 309, 106605. doi:10.1016/j.pepi.2020.106605
- Schnepf, E., Thallner, D., Arneitz, P., Mauritsch, H., Scholger, R., Rolf, C., et al. (2020b). New archaeomagnetic secular variation data from Central Europe. I: directions. *Geophys. J. Int.* 220 (2), 1023–1044. doi:10.1093/gji/ggaa492
- Smirnov, A. V., Kulakov, E. V., Foucher, M. S., and Bristol, K. E. (2017). Intrinsic paleointensity bias and the long-term history of the geodynamo. *Sci. Adv.* 3 (2), e1602306. doi:10.1126/sciadv.1602306
- Song, Y. X. (2008). *Tiangong kaiwu (in Chinese)*. Shanghai Rarebooks Publishing House.
- Wang, F.-G., Yang, S.-X., Ge, J.-Y., Ollé, A., Zhao, K.-L., Yue, J.-P., et al. (2022). Innovative ochre processing and tool use in China 40,000 years ago. *Nature* 603 (7900), 284–289. doi:10.1038/s41586-022-04445-2
- Wang, Q., Gong, Z., Victor, S. K., Corolla, M., Underhill, A. P., McIntosh, R. J., et al. (2023). New archaeomagnetic directions from Late Neolithic sites in Shandong province, China. *Geophys. J. Int.* 232 (2), 1159–1172. doi:10.1093/gji/ggac381
- Wei, Q., Li, D., Cao, G., Zhang, W., and Wang, S. (1980). ARCHAEOMAGNETIC RESEARCH OF JIANGZHAI RELIC, NEOLITHIC EPOCH. *Chin. J. Geophys. (In Chinese)* 23 (04), 403–414.
- Xu, S., and Dunlop, D. J. (2004). Thellier paleointensity theory and experiments for multidomain grains. *Journal of Geophysical Research Solid Earth* 109 (B7). doi:10.1029/2004JB003024
- Yang, Y., Yu, S.-Y., Zhu, Y., and Shao, J. (2014). The making of fired clay bricks in China some 5000 Years ago. *Archaeometry* 56 (2), 220–227. doi:10.1111/arc.12014
- Zhang, Q., and Appel, E. (2023). Reversible thermal hysteresis in heating-cooling cycles of magnetic susceptibility: a fine particle effect of magnetite. *Geophysical Research Letters* 50 (6), e2023GL102932. doi:10.1029/2023GL102932
- Zhao, P., Zhang, X., Qin, L., Zhang, Y., and Zhou, L. (2019). Conservation of disappearing traditional manufacturing process for Chinese grey brick: field survey and laboratory study. *Construction and Building Materials* 212, 531–540. doi:10.1016/j.conbuildmat.2019.03.317
- Zijderveld, J. D. A. (2013). A. C. Demagnetization of rocks: analysis of results. *Developments in Solid Earth Geophysics* 3, 254–286. doi:10.1016/B978-1-4832-2894-5.50049-5